
A High-Energy, High-Average-Power Laser Using Nd:YLF Rods Corrected by Magnetorheological Finishing

Introduction

Optical parametric chirped-pulse amplification^{1,2} (OPCPA) is well suited for the front end of modern petawatt glass laser chains.³ The broadband gain available with OPCPA at a wavelength of 1053 nm offsets the gain narrowing that occurs in large Nd-doped glass amplifiers.⁴ It can be scaled to large energies,⁵ in contrast to the practical limits imposed by the mode volume of a laser cavity in regenerative amplification. Lastly, the OPCPA process is prepulse free⁶ and can produce gains of up to 10^9 using a relatively simple optical system, which minimizes beam distortions.

Recently, we have shown that a high conversion efficiency of 30% and stable output energies⁷ can be achieved in an OPCPA system using pump-laser pulses with uniform intensity profiles in both space and time. This significantly reduces the pump-laser energy requirements. Following this approach, an OPCPA system design⁸ was proposed to amplify chirped pulses to more than 400 mJ while limiting the pump-laser requirement to approximately 1 J at a wavelength of 527 nm.

Several laser-amplifier architectures are capable of producing high pump-pulse energies. High-energy, Q -switched, unstable laser oscillators are commercially available and involve a relatively simple setup, but spatiotemporal coupling in the pump pulse limits the useful energy ultimately available for the OPCPA process, which in turn limits OPCPA conversion efficiency.⁹ Master-oscillator, power-amplifier (MOPA) schemes utilizing amplifiers with progressively larger apertures cause large square-pulse distortions that pose a significant challenge when a temporally square output pulse is desired. More generally, amplification schemes that conjugate both high gain and large depletion of the gain medium limit the ability to control the pump-laser parameters. On the contrary, multipass geometries that utilize the full aperture of a gain medium avoid this difficulty since heavy gain saturation occurs only in the final passes. Multipass amplifiers also offer more-compact layouts and reduce pumping system complexity compared to linear MOPA systems.

Various active and passive multipass architectures offer unique advantages and disadvantages. Passive schemes with Faraday isolators or quarter-wave plates provide the simplest operational scheme but limit the number of passes in the gain medium. The number of passes in linear¹⁰ and ring¹¹ laser-amplifier cavities can be selected by timing the Q -switching and cavity dumping with an intracavity Pockels cell, although this increases operational complexity. Angular multiplexing¹² eliminates the need for active switching but, as a result, is a less-flexible technique.

A limited number of gain media are suitable for high-energy laser applications. Among them, Nd:YAG was considered but not selected because of its high-stimulated emission cross section (low stored-energy density) and poor thermal behavior characteristics, such as a high thermal lensing effect and a high thermally induced stress birefringence. Nd:YLF operating at 1053 nm provides several advantages: First, a high saturation fluence (low-gain cross section) allows working at high laser fluence while minimizing pulse distortion. Second, strong static birefringence practically eliminates the impact of thermally induced stress birefringence, and Nd:YLF has a relatively weak thermal astigmatism. A final practical advantage is that it matches the gain peak of Nd-doped phosphate laser glasses, which permits employing a common front end for both pumping OPCPA systems and seeding large glass amplifiers used in large laser-fusion facilities. Unfortunately, the transmitted-wavefront quality of commercially available, large-aperture Nd:YLF laser rods was not previously sufficient for pumping an OPCPA system.

This article describes a multijoule laser amplifier based on a crystal large-aperture ring amplifier (CLARA) that is capable of producing high-energy pulses with the parameters required for a highly efficient OPCPA. The CLARA design uses 25.4-mm-diam Nd:YLF rods that can operate at a 5-Hz repetition rate because of their good thermal properties. Surface figure corrections were polished on one face of each CLARA rod using magnetorheological finishing (MRF)¹³ to

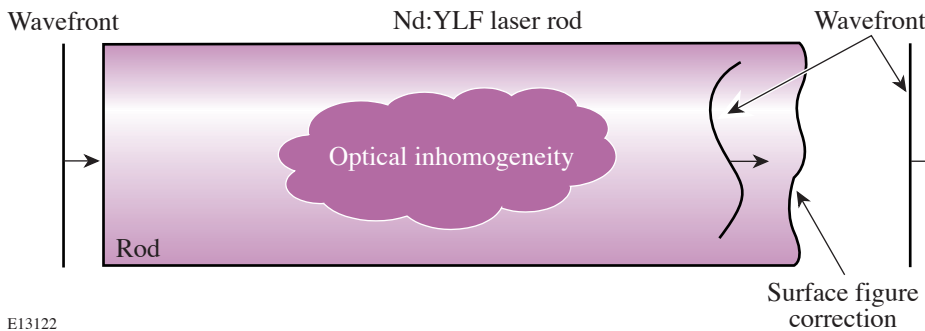
compensate for the bulk inhomogeneities that cause the transmitted-wavefront errors. Correcting these errors increases the usable aperture of the Nd:YLF laser rods, which consequently increases the energy extraction from the laser rods. To our knowledge, this is the first reported application of MRF processing to correct the transmitted wavefront of a laser gain material.

The following sections (1) present the process and experimental realization of correcting the transmitted wavefront of a Nd:YLF laser; (2) describe the design of the CLARA laser amplifier, including an interferometric alignment technique that ensures that the MRF-corrected laser rods are properly aligned; (3) present experimental results demonstrating the benefits of the MRF correction on amplifier performance; and (4) discuss the potential applications of MRF to crystal laser material.

Magnetorheological Finishing of Nd:YLF Rods

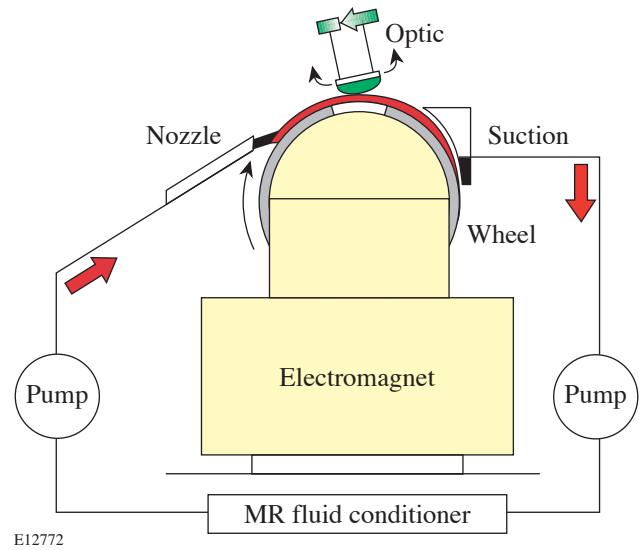
Nd:YLF rods that are 25 mm in diameter represent the state of the art in crystal growth. Growing these laser rods with high optical-wavefront quality is extremely challenging, if not impossible. Even with the end-faces polished perfectly flat, up to several microns of wavefront distortion in the bulk crystal is typical. This makes these rods unsuitable for use in a high-energy laser system because these phase errors quickly turn into hot spots as the beam propagates. Additionally, large phase gradients introduced by the rod aberrations produce a beam divergence that phase-matches poorly in nonlinear optical processes, such as frequency doubling and OPCPA.

To overcome these limitations, surface figure corrections can be polished on one face of a laser rod using MRF to compensate for the bulk inhomogeneities that cause the transmitted wavefront errors, as shown schematically in Fig. 99.63. Correcting these errors increases the usable aperture of the Nd:YLF laser rods, which consequently increases the energy extraction.



E13122

The MRF process utilizes a small polishing spot formed on a rotating wheel carrying a ribbon of magnetorheological (MR) fluid that contains polishing abrasive, as shown in Fig. 99.64. As the ribbon of MR fluid passes between the poles of a powerful electromagnet, the MR fluid viscosity increases and distributes the polishing abrasive at the surface of the ribbon, where it produces a deterministic, two-dimensional removal-rate pattern. Once the removal-rate function for a material is characterized, a prescribed surface figure correction can be achieved by controlling the dwell time of the optic at each point on the surface as it moves under the wheel in



E12772

Figure 99.64 MRF principle. The MRF fluid is pumped to a rotating wheel that passes between the poles of a powerful electromagnet. In the magnetic field, the MRF fluid viscosity increases to a nearly solid consistency, which forms a sub-aperture polishing tool. After passing through the electromagnet, the MRF fluid is reconditioned and recycled.

Figure 99.63 Transmitted-wavefront errors induced by bulk inhomogeneities in a Nd:YLF laser rod can be compensated by polishing a surface figure correction on one end-face of the rod.

either a raster or spiral pattern. Interferometry prior to an MRF polishing step measures the actual wavefront error of the sample, which is used to compute the MRF correction. Wavefront corrections converge quickly, usually requiring no more than two or three iterations.

Figure 99.65 shows the results of correcting a Nd:YLF laser rod. Initially, the transmitted-wavefront error for this laser rod was 0.60λ (at 1053 nm) in the desired 20-mm clear aperture. After several MRF iterations, this error was reduced to 0.11λ . Table 99.III summarizes the results of correcting five different laser rods. Final wavefronts of $\sim \lambda/10$ were generally achieved, except when the spatial structure of the initial wavefront error approached or exceeded the resolution of the MRF correction process.

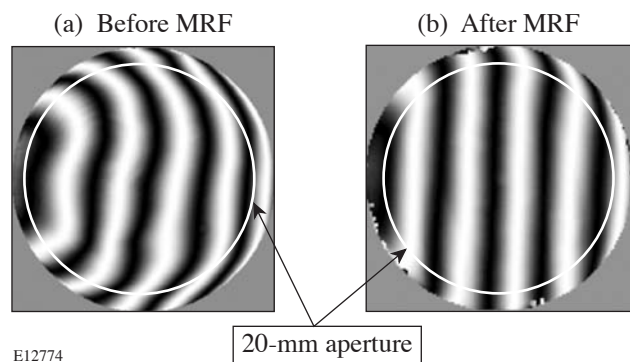


Figure 99.65 Interferograms for rod 2 show the transmitted-wavefront error (a) before and (b) after MRF correction. MRF corrections were applied to the central, 20-mm-diam circular region of the laser rod. The wavefront error was reduced from 0.60λ to 0.11λ (peak-to-valley at 1053 nm).

Table 99.III: Transmitted-wavefront distortion of 25-mm-diam Nd:YLF rods before and after MRF correction.

Rod number	Wavefront before MRF (peak-to-valley) in waves at 1053 nm	Wavefront after MRF (peak-to-valley) in waves at 1053 nm
Rod 0	3.9λ	0.06λ ($15 \times 15 \text{ mm}^2$)
Rod 1	1.5λ	0.16λ
Rod 2	0.60λ	0.11λ
Rod 3	0.92λ	0.10λ
Rod 4	3.2λ	0.10λ (18-mm diam)

Several issues associated with wavefront-correcting Nd:YLF laser rods were identified: First, the measured transmitted-wavefront distortion in Nd:YLF is different for linearly polarized light aligned with the *c* axis (1047 nm) or *a* axis (1053 nm). As a result, MRF corrections are required for the specific polarization used for laser operation.

Second, the transmitted-wavefront quality of MRF-corrected laser rods depends on its alignment. Transmitted-wavefront error of a laser rod results from the accumulation of different optical phase delays across the aperture in the propagation direction. Since MRF corrections are applied on a single end-face to correct for bulk inhomogeneities distributed throughout the laser rod, the operational alignment of a corrected rod must match that used for the interferometric measurement upon which the MRF correction is applied. The orientation of the laser rod during the interferometry measurements of successive MRF iterations must be repeatable for the corrections to converge. This alignment repeatability ultimately limits the residual wavefront error that can be achieved, which depends on the initial wavefront error.

Figure 99.66 shows the measured alignment sensitivity of three MRF-corrected laser rods. The transmitted-wavefront error was measured as a function of rod orientation using a Zygo GPIxps interferometer. The rods were first aligned with a tip-tilt stage to achieve the minimum transmitted-wavefront error, corresponding to the MRF-correction alignment orientation. The peak-to-valley transmitted-wavefront error was measured for a range of misalignment angles. Transmitted-wavefront errors better than $\lambda/4$ were obtained for angular misalignment of rods #2 and #3 not exceeding ± 10 mrad, while a narrower range of ± 4 mrad was observed for rod #4 since its initial wavefront quality was poorer. Given that alignment accuracy better than ± 1 mrad can be achieved by standard alignment techniques, diffraction-limited performance is expected.

It is important to note that the MRF-correction process cannot address transmitted amplitude distortions that can arise from inclusions or scattering sites in the bulk material, or depolarization in a polarization-sensitive scheme such as a *Q*-switched laser cavity. To avoid these problems, a careful selection of the best Nd:YLF boules is required.

Experimental Setup

The laser system, including both the low-energy front end and the CLARA amplifier, is presented schematically in Fig. 99.67. Seed pulses are generated in a diode-pumped,

single-longitudinal-mode Nd:YLF laser¹⁴ producing ~100-nJ, 100-ns pulses at 1053 nm at a 300-Hz repetition rate. The output of the oscillator is temporally shaped using an aperture-coupled-strip-line (ACSL) pulse-shaping system¹⁵ that precompensates for the square-pulse distortion occurring in the amplifier. Timing jitter of this pulse shape with respect to an external timing reference signal is approximately 15-ps rms. The temporally shaped pulse is subsequently amplified

from ~50 pJ to 3 mJ in a diode-pumped, Nd:YLF regenerative amplifier.¹⁶ In addition to providing excellent spatial beam quality and energy stability, square-pulse distortion in this amplifier is relatively weak (0.8:1), which minimizes the dynamic range requirements of the pulse-shaping system. After the regenerative amplifier, the laser beam is up-collimated to 15 mm (FWHM) before spatially shaping the beam to a super-Gaussian profile with a serrated-tooth apodizer.¹⁷

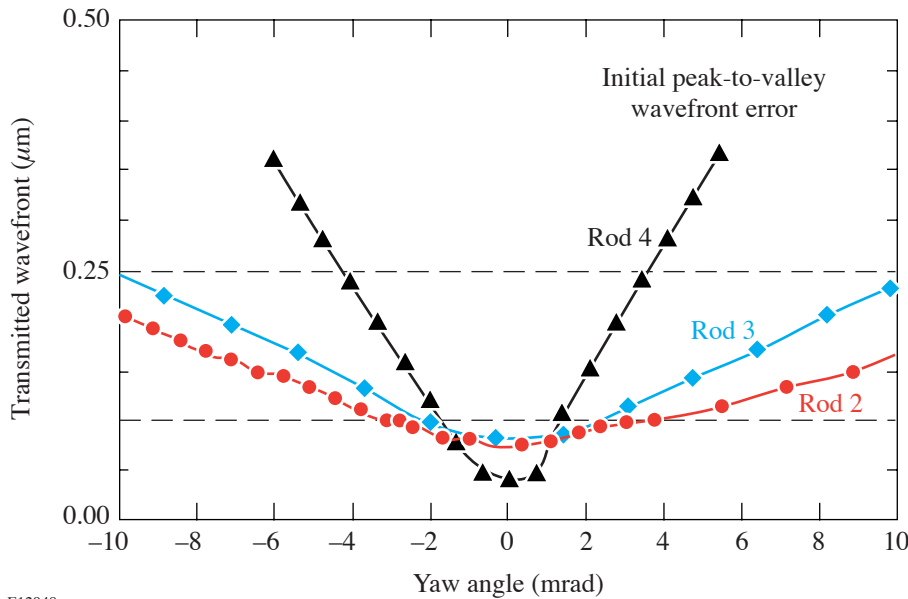
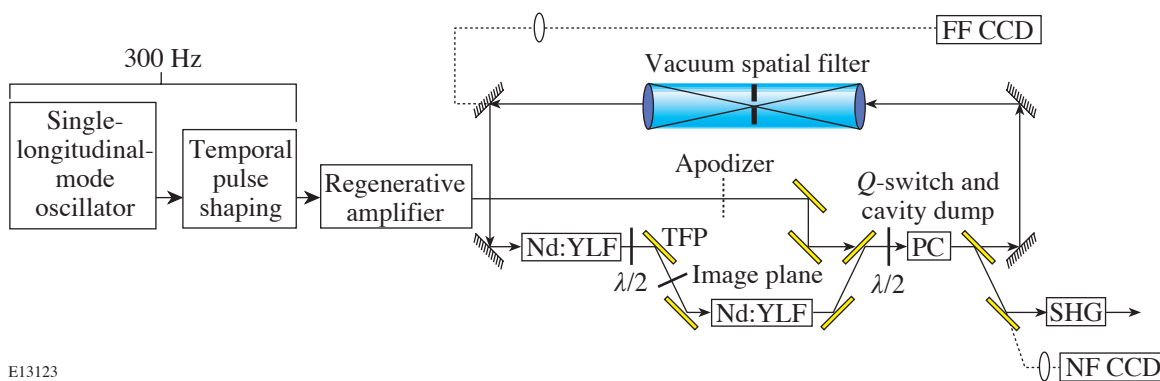


Figure 99.66 The transmitted-wavefront error of MRF-corrected rods is sensitive to its orientation. Optimum performance is achieved when the alignment matches the orientation used during measurements to perform the MRF correction. Increased alignment sensitivity is observed for rods with larger initial wavefront errors.

E12948



E13123

Figure 99.67 Experimental setup. The low-energy part includes a single-longitudinal-mode oscillator, the pulse-shaping system, and the regenerative amplifier. The CLARA setup includes the serrated-tooth apodizer, the CLARA ring, alignment cameras (NF CCD and FF CCD), and the frequency-conversion crystal. TFP: thin-film polarizer; SHG: frequency-doubling crystal; PC: Pockels cell; $\lambda/2$: half-wave plate.

Amplification to high pulse energies is accomplished using a CLARA amplifier, shown in Fig. 99.67. The CLARA architecture is based on a Q -switched, cavity-dumped, self-imaging laser cavity. After the pulse is injected through the intracavity Pockels-cell switch, the external apodizer location is imaged to a location between the two laser rods by a telephoto vacuum spatial filter. The spatial filter also image-relays the beam through successive round-trips in the cavity. Two 110-mm-long, 25.4-mm-diam, Nd:YLF, MRF-corrected laser rods are loaded into custom flash-lamp-pumped heads from Continuum with four flash lamps that achieve a single-pass small signal gain of approximately $3\times$ per head. A pair of thin-film polarizers optically isolate the two laser heads to avoid parasitic lasing of the system on the higher-gain, 1047-nm gain transition. Orienting the 1053-nm gain axes of the two Nd:YLF laser rods at 90° cancels residual thermal astigmatism, leaving only a weak defocus that is easily accommodated by the beam-transport system. A 25.4-mm-aperture Pockels cell Q -switches the laser cavity and sets the number of round-trips in the 7-m (21-ns) round-trip cavity.

As described above, an MRF-corrected laser rod must be operated with an orientation identical to that used for the correction process. This is achieved by using an interferometric alignment technique for the CLARA laser system that will minimize the total accumulated wavefront error per round-trip through the CLARA. To measure the CLARA transmitted wavefront, an interference pattern is generated between the CLARA output beam and the reference beam. A CCD (charge-coupled-device) camera that images the CLARA image plane (labeled NF CCD in Fig. 99.67) records the interference pattern. Wavefront retrieval is achieved by applying a spatial interferometric technique¹⁸ based on the analysis of tilt fringes and implemented for real-time operation. To produce the reference beam, a half-wave plate is placed in the CLARA, just before the Pockels cell, splitting the laser beam into two beams. This wave plate (shown in Fig. 99.67) is usually removed during operation of the CLARA. One beam propagates through the CLARA and is ejected at the next pass on the polarizer; the other beam, which does not go through the CLARA, is used as a reference beam. In addition to spatial overlap, temporal overlap of the laser pulses is required to have a visible interference pattern. Practically, two output pulses are produced from the regenerative amplifier by intentionally mistiming the cavity dumping. Since the round-trip times of the CLARA and regenerative amplifier are nearly identical, a pulse that travels one round-trip inside the CLARA temporally overlaps with the following pulse on the thin-film polarizer used for injecting the pulses. With temporal and spatial over-

lap, the interference pattern can be seen in the near field. By adjusting the half-wave plate, the interference fringes' contrast is maximized. A LabVIEW image acquisition and analysis utility records the interference pattern and retrieves the wavefront error in real time. Using this measurement technique, the lens separation in the spatial filter is adjusted with submillimeter accuracy, and the MRF-corrected laser rods can be aligned with great accuracy.

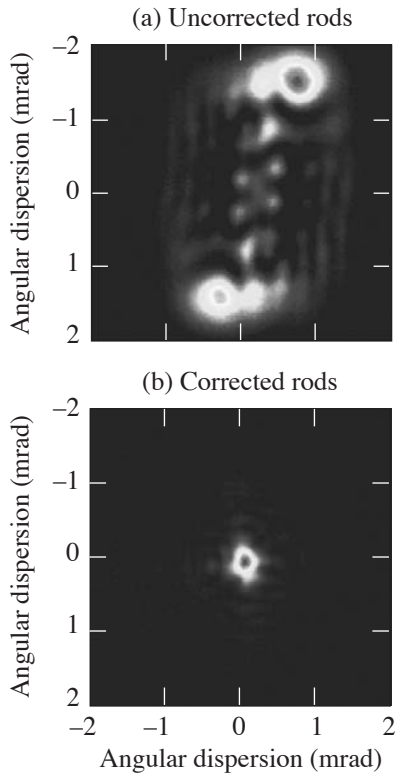
A simple three-dimensional amplification model, based on the Frantz–Nodvik equation,¹⁹ was used to optimize the CLARA. The finite lifetime of the lower level of the Nd:YLF, 1053-nm lasing transition is treated by assuming that the system behaves as a three-level system at each pass, but with exponential decay of the lower-level population between round-trips. Given a lower-level decay time of 21.6 ns (Ref. 20), a pulse of 2 ns, and a round-trip time of 21 ns, we believe the approximation is valid. The model predicts that best energy extraction is achieved for five or six round-trips for a small signal gain of 4 and 3 per rod, respectively, and an injected energy of about 1 mJ. The more round-trips, however, the more wavefront distortion, so we decided to operate the system with four round-trips, where the energy extraction is lower but wavefront distortion is minimized. In addition, less saturation also means lesser distortion of the pump-laser parameters.

After amplification in the CLARA with four round-trips, a second spatial filter down-collimates the beam to a $15 \times 15\text{-mm}^2$ -aperture, 10-mm-thick-lithium-triborate (LBO), second-harmonic-generation (SHG) crystal with a nominal incident intensity of 1 GW/cm^2 .

Results

Results from operating the CLARA with a 10-mm round beam and uncorrected Nd:YLF laser rods are shown in Fig. 99.68. The figure shows the intensity distribution of the beam in the far field at the OPCPA crystal, where its diameter has been reduced to roughly 2 mm. The measured far field shows a large angular divergence that is unsuitable for pumping phase-matched processes like SHG and OPCPA. Inversion symmetry observed in this image results from the inverted imaging produced by the intracavity spatial filter. As a result, the spatial phase function of the beam is symmetrical, leading to a symmetrical energy distribution in the far field. Figure 99.68(b) shows the corresponding CLARA far-field measurement using MRF-corrected laser rods, which illustrates the greatly improved divergence of this beam. Unfortunately, MRF corrections for these Nd:YLF laser rods were not applied for the correct polarization corresponding to the 1053-nm gain

transition; nonetheless, a dramatic reduction in the angular divergence is realized.



E13124

Figure 99.68 Pump-laser far-field distribution measured for a 2-mm beam used to pump an OPCPA preamplifier. (a) The divergence of the beam using uncorrected Nd:YLF rods is large and unsuitable for SHG and OPCPA. (b) Nearly diffraction limited divergence is achieved after MRF correcting the CLARA rods, although some residual divergence results from correcting the transmitted wavefront of the wrong polarization.

This improvement in the Nd:YLF laser rod quality increases the usable clear aperture and the stored energy available for extraction. Without MRF-corrected rods, it should be stressed that a 10-mm beam was the largest-diameter beam that could propagate through the amplifier without suffering huge spatial modulation or distortion. Figure 99.69 compares the CLARA output beam profile before and after the MRF correction for a similar input beam. The beam injected into the amplifier is limited by a circular tenth-order super-Gaussian apodizer that sets a 10-mm diameter (FWHM). The beam in Fig. 99.69(a) shows some important spatial distortion, which illustrates the maximum beam diameter that the system could support. The beam in Fig. 99.69(b) shows very little distortion, while the peak-to-mean value of the beam is improved from

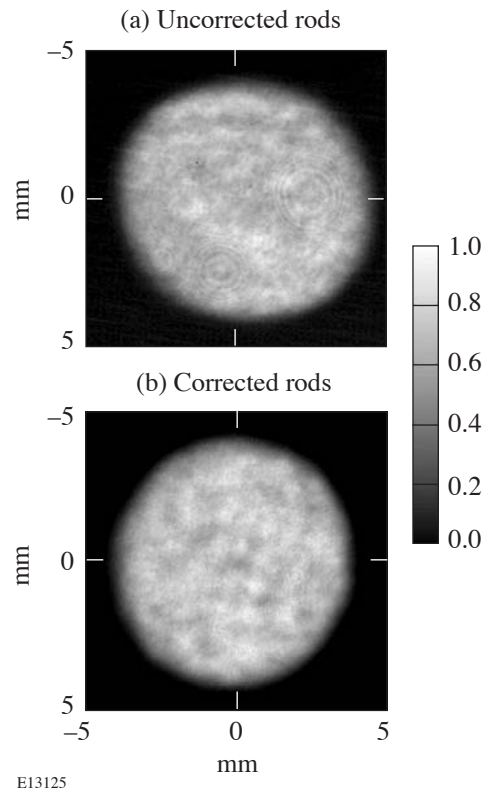


Figure 99.69 Near-field images of the laser beam, at 2ω , after frequency conversion. The dimensions reflect the beam size at this location, which is different from the beam size in the CLARA. (a) CLARA output beam with uncorrected rods and (b) CLARA output beam with MRF-corrected rods.

49% to 41%. Except for beam distortion, which is important for an OPCPA system used as the front end of a larger system, the improvement in the near field is marginal, as may be expected for an imaged system.

The amplifier with MRF-corrected rods can amplify beams with a much larger area. Figure 99.70 shows spatial profiles of two larger beams amplified in the CLARA, when both (a) a round 17-mm-diam apodizer and (b) a square 14-mm-diam apodizer are used. The corresponding measured energies at 527 nm are 1.4 and 1.8 J, respectively, for a maximum average power of 9 W. In all cases, the SHG conversion efficiency using MRF-corrected rods exceeds 70%. The beam-intensity uniformity is 90% and 92% peak-to-mean for the round and square beams, respectively. The poorer beam-intensity uniformity could be explained by a beam extending slightly beyond the useful area of the rods and a poor matching of the input beam on the apodizer since the system was optimized for smaller-diameter beams. By carefully optimizing the input

beam diameter such that radial gain inversely matches the input beam's Gaussian shape at the apodizer, we believe near-top-hat conditions could be achieved.

The energy stability of the laser is remarkable. For instance, with large round beams, the energy stability is smaller than 0.5% rms over a 10,000-shot count at 5 Hz, as shown in Fig. 99.71 by the pulse energy versus shot number and the corresponding pulse-energy histogram. This excellent result for a flash-lamp-pumped system is attributed to the stable CLARA seed-pulse energy provided by the diode-pumped regenerative amplifier, strong simmering of the flash lamps, and heavy saturation of the SHG process.

Discussion and Conclusion

The transmitted wavefront of a laser gain material has been corrected for the first time by magnetorheological finishing. Polishing a surface figure correction with MRF directly on one surface of 25.4-mm-diam Nd:LF laser rods compensates for bulk inhomogeneities. The results show a dramatic increase in the energy and wavefront-quality performance of the CLARA laser amplifier. The CLARA amplifier demonstrates a high average power of 9 W, which could be increased by 20% to 30% by increasing the number of passes in the amplifier and using laser rods with wavefront corrections correctly applied for the 1053-nm polarization.

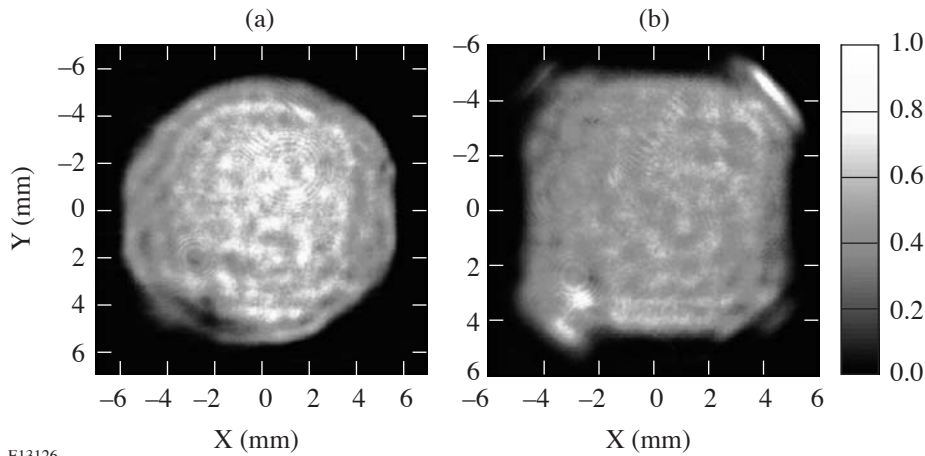
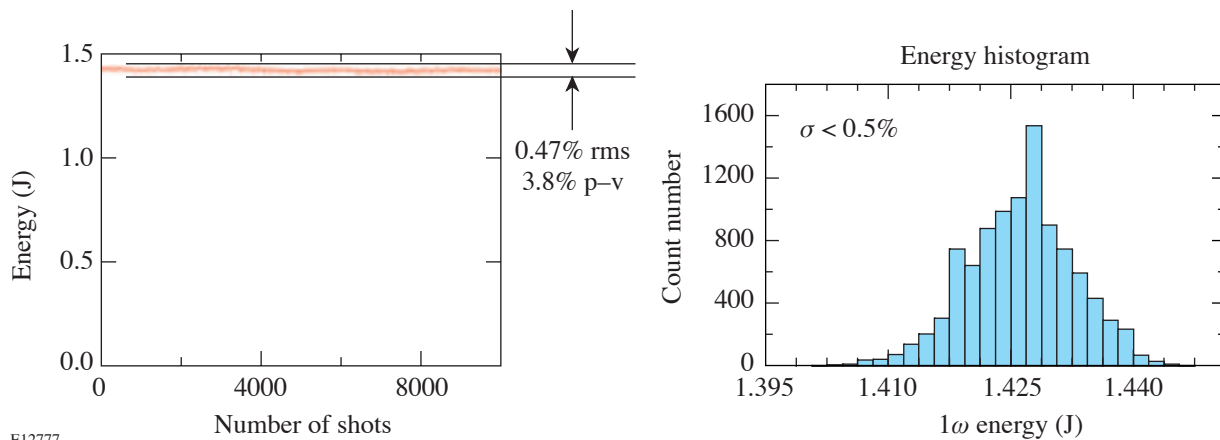


Figure 99.70
Larger beams can be amplified in the CLARA with MRF-corrected laser rods. Results with (a) a round, 17-mm-diam and (b) a square, 14-mm, 20th-order Gaussian spatial profile are demonstrated.

E13126



E12777

Figure 99.71
Energy stability at the output of the laser.

The MRF technique holds promise for additional applications, such as precompensating thermal aberrations and post-processing large-area laser crystals. Numerous techniques have been reported to mitigate thermal lensing in materials like Nd:YAG.^{21,22} Since thermal lensing is a low-order error to the transmitted wavefront, MRF corrections to laser gain elements should easily statically precompensate for it without requiring any other elements in the laser cavity. It should be noted that MRF is probably not well-suited to small rods since edge effects and the finite MRF spot size become a problem with small areas. Efforts to produce large-area crystals of Yb:SFAP and Ti:sapphire are being pursued by diffusion bonding of smaller-aperture elements, but the transmitted-wavefront distortions are observed at the boundaries in such crystals. MRF wavefront corrections might solve this problem, as long as the wavefront gradients are not excessive.

In conclusion, use of a high-energy, high-average-power laser that is suitable for pumping an OPCPA-based front end for a petawatt laser system is demonstrated. Early results show a system that delivers 250-mJ pulses with 34% pump-to-signal energy conversion efficiency with a 10-mm round CLARA beam. This shows that the laser system is well suited to efficiently pumping a high-average-power OPCPA system. Further experiments are underway to use the full CLARA aperture and deliver >500-mJ OPCPA pulses.

ACKNOWLEDGMENT

The authors thank VLOC for providing the Nd:YLF samples used to characterize the MRF process. This work was supported by the U.S. Department of Energy Office of Inertial Confinement Fusion under Cooperative Agreement No. DE-FC52-92SF19460, the University of Rochester, and the New York State Energy Research and Development Authority. The support of DOE does not constitute an endorsement by DOE of the views expressed in this article.

REFERENCES

1. A. Dubietis, G. Jonusauskas, and A. Piskarskas, *Opt. Commun.* **88**, 437 (1992).
2. I. N. Ross *et al.*, *Opt. Commun.* **144**, 125 (1997).
3. H. Yoshida *et al.*, *Opt. Lett.* **28**, 257 (2003).
4. J. Collier *et al.*, *Appl. Opt.* **38**, 7486 (1999).

5. J. L. Collier *et al.*, "Progress Towards Petawatt Level OPCPA," to be published in *Inertial Fusion Sciences and Applications 2003*.
6. Y. Kitagawa *et al.*, *IEEE J. Quantum Electron.* **40**, 281 (2004).
7. L. J. Waxer, V. Bagnoud, I. A. Begishev, M. J. Guardalben, J. Puth, and J. D. Zuegel, *Opt. Lett.* **28**, 1245 (2003).
8. M. J. Guardalben, J. Keegan, L. J. Waxer, V. Bagnoud, I. A. Begishev, J. Puth, and J. D. Zuegel, *Opt. Express* **11**, 2511 (2003).
9. I. Jovanovic *et al.*, *Appl. Opt.* **41**, 2923 (2002).
10. V. Bagnoud, J. Luce, L. Videau, and A. Rouyer, *Opt. Lett.* **26**, 337 (2001).
11. A. Babushkin, J. H. Kelly, C. T. Cotton, M. A. Labuzeta, M. O. Miller, T. A. Safford, R. G. Roides, W. Seka, I. Will, M. D. Tracy, and D. L. Brown, in *Third International Conference on Solid State Lasers for Application to Inertial Confinement Fusion*, edited by W. H. Lowdermilk (SPIE, Bellingham, WA, 1999), Vol. 3492, pp. 939–943.
12. C. Le Blanc *et al.*, *Opt. Lett.* **18**, 140 (1993).
13. D. Golini, S. Jacobs, W. Kordonski, and P. Dumas, in *Advanced Materials for Optics and Precision Structures*, edited by M. A. Ealey, R. A. Paquin, and T. B. Parsonage, *Critical Reviews of Optical Science and Technology* (SPIE, Bellingham, WA, 1997), Vol. CR67, pp. 251–274.
14. A. V. Okishev and W. Seka, *IEEE J. Sel. Top. Quantum Electron.* **3**, 59 (1997).
15. M. D. Skeldon, *Rev. Sci. Instrum.* **71**, 3559 (2000).
16. A. V. Okishev, D. J. Battaglia, I. A. Begishev, and J. D. Zuegel, in *OSA TOPS Vol. 68, Advanced Solid-State Lasers*, edited by M. E. Fermann and L. R. Marshall, *OSA Technical Digest* (Optical Society of America, Washington, DC, 2002), pp. 418–422.
17. J. M. Auerbach and V. P. Karpenko, *Appl. Opt.* **33**, 3179 (1994).
18. M. Takeda, H. Ina, and S. Kobayashi, *J. Opt. Soc. Am.* **72**, 156 (1982).
19. L. M. Frantz and J. S. Nodvik, *J. Appl. Phys.* **34**, 2346 (1963).
20. J. D. Zuegel and W. Seka, *IEEE J. Quantum Electron.* **31**, 1742 (1995).
21. G. Vdovin and V. Kiyko, *Opt. Lett.* **26**, 798 (2001).
22. R. Weber, T. Graf, and H. P. Weber, *IEEE J. Quantum Electron.* **36**, 757 (2000).

